SYNERGY OF OPTICAL AND SYNTHETIC APERTURE RADAR (SAR) SATELLITE IMAGES FOR MAPPING POST-FLOOD RICE CROPLAND RECOVERY: A CASE STUDY IN KITCHARAO, AGUSAN DEL NORTE PHILIPPINES

Wesley T. Clifford[1], Pia Lauritz A. Bocboc[2], Arturo G. Cauba Jr.*[3] and Monalaine M. Bermoy4
[1]Undergraduate Student, Department of Geodetic Engineering, Caraga State University
Ampayon, Butuan City, Philippines
Email: dispowesleyclifford@gmail.com

[2]Undergraduate Student, Department of Geodetic Engineering, Caraga State University
Ampayon, Butuan City, Philippines
Email: pialauritzazarcon@gmail.com

[3]Faculty member, Department of Geodetic Engineering, Caraga State University
Ampayon, Butuan City, Philippines
Email: agcauba@carsu.edu.ph

[4]Faculty member, Department of Geodetic Engineering, Caraga State University
Ampayon, Butuan City, Philippines
Email: mmbermoy@carsu.edu.ph

KEY WORDS: Binarization, Flood Recovery, Sentinel-1, Sentinel-2, Thresholding

ABSTRACT: Natural disasters such as floods can significantly impact agriculture, especially in rice crop areas. The synergy of optical and synthetic aperture radar (SAR) images can be utilized to monitor post-flood rice crop recovery. This study investigates the potential of using optical and SAR images to monitor rice crop recovery after a flood event in Kitcharao, Agusan del Norte. The study utilizes optical images from Sentinel-2 and SAR images from Sentinel-1. The images were pre-processed and then subjected to manual thresholding and layer stacking techniques to generate rice crop extent maps and flood maps. The accuracy of the rice crop maps and flood map was evaluated using the confusion matrix and kappa coefficient. The results revealed that only 2.25% of the rice crops survived a week after the flooding, indicating the extent of the damage caused by the flood. Furthermore, the recovery rate of rice crops after a month was only 8.89%, indicating that the damage caused by the flood had long-lasting effects on the crops. The study demonstrates the potential of using remote sensing techniques to monitor post-flood rice crop recovery and the importance of combining optical and SAR images for more accurate assessments.

1. INTRODUCTION

1.1 Background of the Study

Agriculture is an essential component in preserving human societies. In addition, agricultural land accounts for approximately forty percent of the total land area on the planet and is continuously expanding (Nguyen et al., 2022). The Philippines has a total agricultural area of 9.67 million hectares, which accounts for approximately 30 percent of the country's total land area and is farmed by around 5 million farmers (Elauria, 2015). The Philippines is one of the countries in Southeast Asia affected frequently by natural disasters such as typhoons, floods, and droughts (Guha- Sapir, D., Below, R., Hoyois, 2015). These natural disasters negatively impact the afflicted areas and the local population in terms of the economy and environment. Moreover, natural disasters continually expose the agriculture and natural resource industries to detrimental effects, rendering them highly vulnerable (Jha et al., 2018). The country's Department of Agriculture has reported that several regions incurred a cost of P37.68 million due to recent flood damage to agriculture (Pinlac, 2022). Floods caused by incessant rainfall have impacted at least 1,559 farmers, devastating 882 metric tons of crops across 1,700 hectares of agricultural land (Pinlac, 2022). The conventional approaches for evaluating the recovery process of agriculture after floods are challenging and costly, impeding the prompt and efficient response to calamities. The utilization of remote sensing technologies presents a viable remedy by facilitating expeditious identification of the scope of flood damage and continuous real-time monitoring of the recovery process (Conde & De Mata Muñoz, 2019). Satellite images and diverse land cover classification techniques have been widely adopted in remote sensing studies to

differentiate and identify specific land cover information (Elauria, 2015; Nguyen et al., 2022). SAR technology in Sentinel-1 satellite data makes it highly advantageous for flood extent mapping due to its ability to operate in all weather conditions, capture images during both day and night and penetrate dense cloud cover (Torres et al., 2017). SAR data with high spatial resolution and dual-polarization backscattering can detect floodwaters and categorize flood-damaged land cover (Conde & De Mata Muñoz, 2019). Conversely, highly detailed spatial data for land cover can be obtained by optical images. Hence, the primary objective of this study is to map the post-flood recovery of rice croplands in the municipality of Kitcharao, Agusan del Norte using Sentinel-1 SAR and Sentinel-2 optical satellite images. Specifically, this study aims to map the extent of rice croplands during pre- and post-flooding using Sentinel-2 data, to assess the post-recovery of rice croplands affected by the mapped flood, and to assess the accuracy and reliability of combining Sentinel-1 SAR and Sentinel-2 optical satellite images in mapping rice crop recovery after a flood event.

1.2 Study Area

Kitcharao, Agusan del Norte, which covers a land area of 128.35 sq. km, consists of 11 barangays that are close to Lake Mainit (PhilAtlas, 2015). Most residents in the area rely on crop farming as their main source of livelihood and economic sustenance. During heavy rainfall, the water level in Lake Mainit rises due to inflows from nearby rivers, which can cause flooding in barangays close to the shoreline. Moreover, the region experienced significant flooding caused by seasonal rainfall in December 2022.

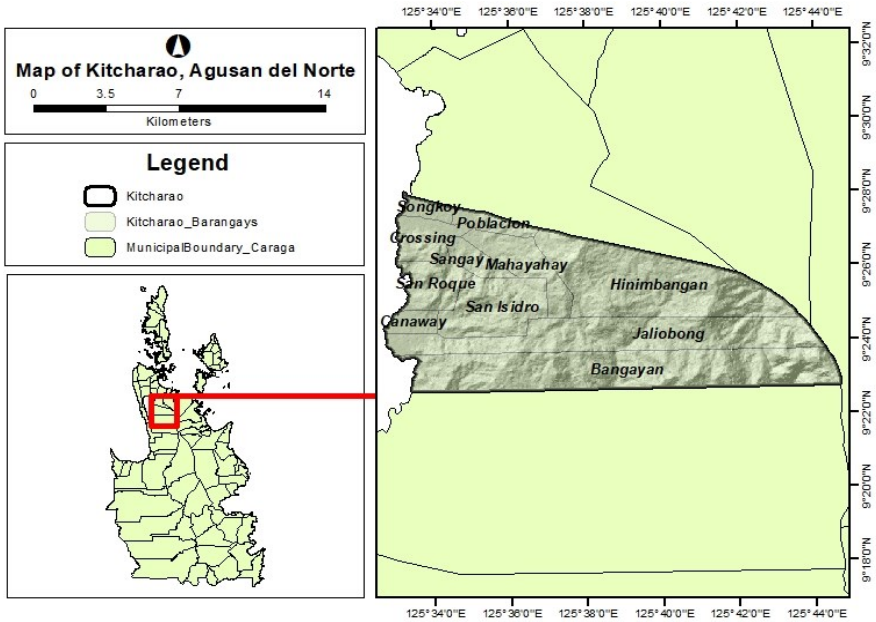

Figure 1.1 Map of the study area

2. MATERIALS AND METHODS

2.1 Dataset

Sentinel-1 SAR data acquired from the Copernicus open-access hub were systematically categorized into three groups: images taken before the inundation incident, images captured at the flood's peak, and images obtained several weeks to months after the flood. Rainfall data for the study area, sourced from the Department of Agriculture, were employed to determine the periods corresponding to the flood's peak event. Consequently, a cross-referencing analysis of the rainfall data and satellite imagery was conducted to accurately determine the periods during which the flood attained its maximum intensity. Sentinel-2 data were integrated to assess the extent of rice crops. In light of a significant flooding event on December 22, 2022, images captured between December 1 and December 22, 2022 were examined to assess the extent of rice crops before the flooding occurred. During the image selection process, priority was given to images with minimal cloud coverage to ensure a more precise and accurate representation of the study area. For the post-flooding analysis, satellite images obtained approximately one week following the flooding event, specifically on January 19, 2023, were utilized to evaluate the condition of the rice crops at that point in time. The purpose of this post-flood image acquisition was to document the immediate aftermath of the event and assess its impact on the rice fields. Additionally, to estimate the yield of the recovered rice crops, satellite images acquired in February 2023, approximately one month after the flood, were analyzed.

To effectively capture and analyze the fluctuations in rice crop extent before, during, and following the flood occurrence, careful selection of satellite images was observed. Tables 2.1 and 2.2 present the sensing period, satellite platform, product type, polarization, and sensor mode of acquired Sentinel-1 and Sentinel-2 satellite images, respectively.

Table 2.1 Metadata of Acquired Sentinel-1 Images

Sensing Period	Satellite Platform	Product Type	Polarization	Sensor Mode
Dec.21, 2022	S1A_*	GRD	VV+VH	IW
Jan. 2, 2023	S1A_*	GRD	VV+VH	IW
Feb 07, 2023	S1A_*	GRD	VV+VH	IW

Table 2.2 Metadata of Acquired Sentinel-2 Images

Sensing Period	Satellite Platform	Product Type
Dec. 12, 2022	S2B_MSIL2A	S2MSI2A
Jan. 16, 2023	S2A_MSIL2A	S2MSI2A
Feb. 25, 2023	S2A_MSIL2A	S2MSI2A

2.2 Methodology

The initial phase entails the identification of areas that are affected by flooding, followed by the continuous monitoring of flood events. The researchers effectively differentiated between inundated and non-inundated regions by utilizing image processing techniques and thresholding methods. This methodology facilitates the observation and evaluation of changes in flood coverage over a period, thereby providing crucial insights into the flooding dynamics of the researched region.

The subsequent step entails the extraction of rice coverage pre- and post-flooding occurrence. We employed remote sensing imagery to capture the spatial distribution of rice crops. The comparative analysis of images taken before and after a flood event enables the detection of regions that have undergone flood-related impacts. This particular step is crucial in obtaining essential information regarding the magnitude of rice loss, which in turn aids in evaluating the overall impact of the flood occurrence on agricultural productivity.

The final step involves conducting accuracy assessments and performing statistical analyses. We thoroughly evaluated the accuracy of flood detection, rice extent mapping, and post-flood recovery approximation. This stage entails comparing the study's findings with ground truth data and utilizing statistical measures to quantify the reliability and precision of the results. The final output of this study is a map that shows the delineation of the regions impacted by flooding and showcases the surviving rice crops following the flood occurrence.

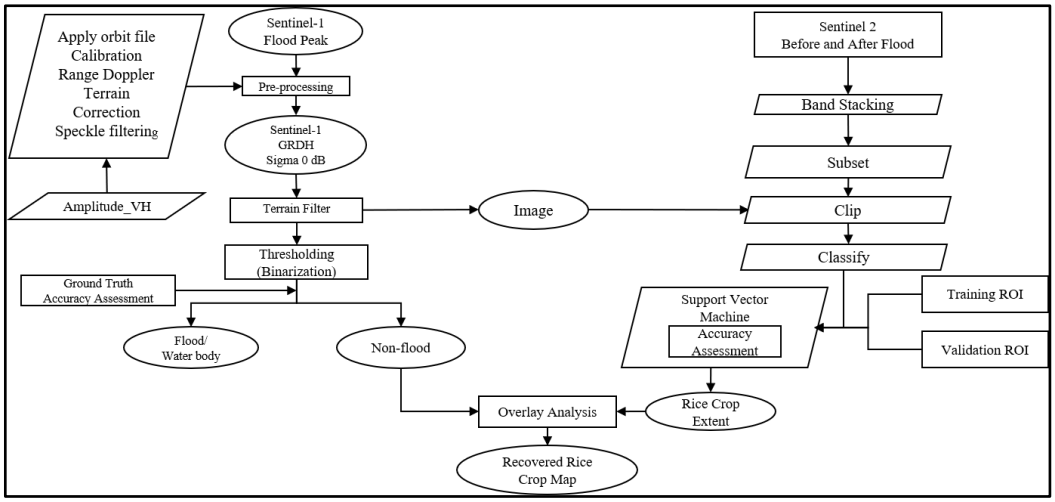

Figure 2.1 Methodology flowchart

2.2.1 Sentinel-1A and Sentinel-2 Pre-processing

We collected Sentinel-1 satellite images before, during the flood peak, and a month after the flooding recedes. The images have undergone pre-processing, i.e. apply orbit file, calibrate, terrain correction/ geometric correction, and speckle filtering, to improve image data by suppressing unwanted noise and distortions and enhancing some image features that are important for future applications. Upon acquiring Sentinel-1A images with VH polarization, Sentinel Application Platform (SNAP) toolkit was used in the preprocessing phase to improve the quality and applicability of the images for subsequent analytical procedures. The SNAP toolkit is used extensively in remote sensing and offers diverse processing capabilities (McGarragh et al., 2015).

Sentinel-2 images with less than 10% cloud coverage were used. The selected images showed an unobstructed perspective of the rice crop's extent before the flood. The satellite images were downloaded using the filtering criteria. ENVI image analysis software was used for processing Sentinel-2 data. The software packages provide various tools and algorithms that enable to manipulate and extract information from satellite imagery (Canty, 2014).

2.2.2 Flood Mapping and Monitoring

Upon obtaining the pre-processed data, we focused on using the images for terrain filtering, thresholding, and accuracy assessment. The process of terrain filtering was implemented to remove extraneous characteristics and highlight the inundated rice fields, thereby facilitating a more accurate demarcation of their perimeters. Subsequently, thresholding techniques were implemented to partition the image and categorize the pixels into regions that are either inundated or non-inundated. The techniques encompass establishing a precise threshold value that discriminates between the two categories based on the backscatter intensity values. We meticulously established the ideal threshold to accurately recognize inundated rice paddies.

For terrain filtering, we generated two datasets, the Height Above the Nearest Drainage (HAND) and the slope, using a Digital Elevation Model (DEM) with a resolution of 10 meters. The terrain filtering process and removing shadowy regions caused by radar interference relied crucially on these datasets. The HAND dataset explains the vertical difference between a pixel and the nearest water channel determined hydrologically. The topographic characteristics of the area are indicated by it, making it a valuable indicator. This study utilized the HAND dataset to identify and exclude topographical sections that were unlikely to be flooded. We combined a slope of 9 degrees with a HAND threshold of 30 meters to create the terrain filter. The radar caused shadowy areas, but the slope component removed them and ensured that further analysis only considered relevant regions. A more detailed DEM with a resolution of 5 meters was used to create the terrain filter. The higher-resolution DEM accurately represented the terrain features. We pre-processed the DEM and performed a series of watershed delineation processes. The pre-processing steps involved removing depressions or inconsistencies in the elevation data by filling sinks, calculating the direction of water flow and the water accumulation in each cell, identifying streams and pour points using the flow accumulation values, and linking the streams to create a continuous network. The delineated watersheds were divided into distinct drainage basins.

The histogram binarization method is an effective approach commonly used in image processing(Wu et al., 2018). The underlying principle of thresholding is predicated on the assumption that there exists an apparent difference in the intensity or color between the objects in the foreground and the background within an image. The process involved the establishment of a threshold value, whereby pixels with intensities or color values surpassing the threshold are categorized as foreground, while those below the threshold are classified as background. The term "histogram-based binarization"

denotes a thresholding technique that relies on the histogram of the image. A histogram is a graphical representation of the distribution of pixel intensities or colors within an image. The process of histogram-based binarization entails examining the histogram in order to identify the most suitable threshold value that can accurately differentiate the foreground from the background. The histogram of the terrain filtered raster image as shown in Figure 2.3 offers a graphical illustration of the occurrence and distribution of pixel values present in the image. The histogram depicts the diversity in terrain attributes that have been extracted through the filtering procedure, facilitating an in-depth assessment of the image's terrain characteristics. Through careful examination of the histogram, significant information can be obtained with regard to the elevation, slope, or other pertinent terrain characteristics that are evident in the filtered raster image. We utilized the histogram of the image to determine an optimal threshold value that maximizes the differentiation between the foreground and background regions. This methodology utilizes the statistical characteristics of the pixel intensities or colors within an image to arrive at a well-informed determination of the threshold values.

We employed the default reclassification tool in ArcGIS to help choose a threshold value and to classify the image. The reclassification tool converted the grayscale image to a binary image by assigning all pixels with intensity values greater than the threshold to white (255) and all other pixels to black (0). This conversion enabled us to differentiate between land and water areas. White areas represented the land, while black areas represented water. This allowed us to identify flooded and non-flooded areas, essential for post-flood recovery assessment. The researchers used the range: min-0.022 (for flooded) and 0.022 to max (for unflooded areas). Figure 2.3 shows the distribution of pixel values of the terrain-filtered Sentinel 1 image, where pixel values with the high frequencies represent the land, and a low pixel value represents the water areas.

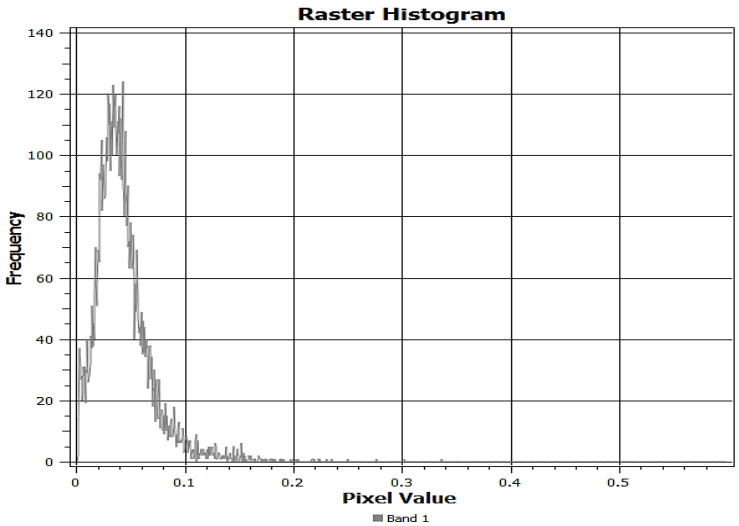

Figure 2.2 Raster Histogram of Terrain Filtered Sentinel-1 Image

2.2.3 In-Situ Observation

To ensure the accuracy of the identified flood areas, we conducted in-situ observations and collected ground coordinates. This involved gathering data directly from the field by physically visiting the study area. We sought assistance from various individuals and stakeholders to obtain ground points representing both flooded and non-flooded areas. Rice field owners, the Department of Agriculture, farmers, and residents played crucial roles in providing valuable information and facilitating the collection of ground coordinates. A combination of interviews and surveys was employed to collect primary data on the scope and geographic distribution of the inundated areas. Reliable and precise data were acquired through direct involvement with the neighbouring community.

Through consultation with the appropriate department, valuable insights were obtained regarding the incidence and extent of flooding in the region. The concern department provided the list of names of the owners of rice fields impacted by flooding. By collaborating with these stakeholders, we were able to obtain firsthand observations and measurements of the actual flooded and non-flooded areas within the study region. The ground coordinates collected through these in-situ observations served as reference points for validating and verifying the accuracy of the flood areas identified through remote sensing techniques. This approach ensured that the analysis and mapping of flood areas were not solely reliant on satellite imagery and computational methods. The integration of ground observations and local knowledge enhanced the reliability and credibility of the research findings, as it involved direct validation against real-world conditions.

2.2.4 Accuracy Assessment

A confusion matrix is a useful tool in classification tasks for evaluating a predictive model's performance. It is a square matrix that shows true positives (TP), true negatives (TN), false positives (FP), and false negatives (FN). This matrix

helps you understand how well your model is doing by comparing predicted labels to actual labels in your dataset. Overall Accuracy tells you the proportion of correctly classified items compared to the total number of items. To calculate accuracy, divide the count of correctly classified items (found on the diagonal of the confusion matrix) by the total number of items and then multiply by 100. Precision, also known as User Accuracy, measures the proportion of correctly classified items in each category relative to the total number of classified items in that category. To calculate precision, divide the count of correctly classified items in each category by the total count of classified items in that category, and then multiply by 100. Producer Accuracy, also called Recall or Sensitivity, quantifies the proportion of correctly classified items in each category relative to the total number of items in that category (the column total). To calculate it, divide the count of correctly identified items in each category by the total count of items in that category and then multiply by 100. Analyzing various metrics from the confusion matrix is essential for interpretation. One such metric is the Kappa coefficient (Cohen's kappa), which measures the agreement between predicted and actual labels while considering chance agreement. The Kappa coefficient ranges from -1 to 1, with different values indicating different levels of agreement. It provides a numeric assessment of agreement beyond what could be due to chance. Higher Kappa values indicate stronger agreement between model predictions and actual labels, while lower values suggest weaker agreement or random predictions. Evaluating these metrics helps assess the reliability of the classification model and the consistency between predicted and actual labels.

2.2.5 Land Cover Mapping

Sentinel-2 satellite imagery was utilized to generate a detailed map of rice cultivation in a specific area. Various spectral bands such as true color, near-infrared, shortwave infrared, and Normalized Difference Vegetation Index (NDVI) were employed for analysis. Specifically, the focus was placed on the near-infrared and red bands with a 10-meter resolution for image processing. The shortwave infrared bands were also subjected to resampling to achieve a 20-meter resolution. The calculation of the NDVI for vegetation assessment was carried out.

To enhance precision, the analysis area was narrowed down, and terrain filtering was applied. A support vector machine (SVM) classifier was trained using labeled samples to classify land cover categories like rice fields. Accuracy metrics (user accuracy and producer's accuracy) were employed to assess classification precision. Contextual editing in ArcGIS software was used to rectify misclassifications, particularly those associated with pixel similarities between rice crops and other vegetation. Various data sources, including in-situ observations and established references, were cross-referenced to ensure unbiased and accurate editing. The resulting land cover map accurately depicted rice farming in the region. Figure 2.3 illustrates the distribution of rice crops in the Caraga Region based on the PhilRice Map.

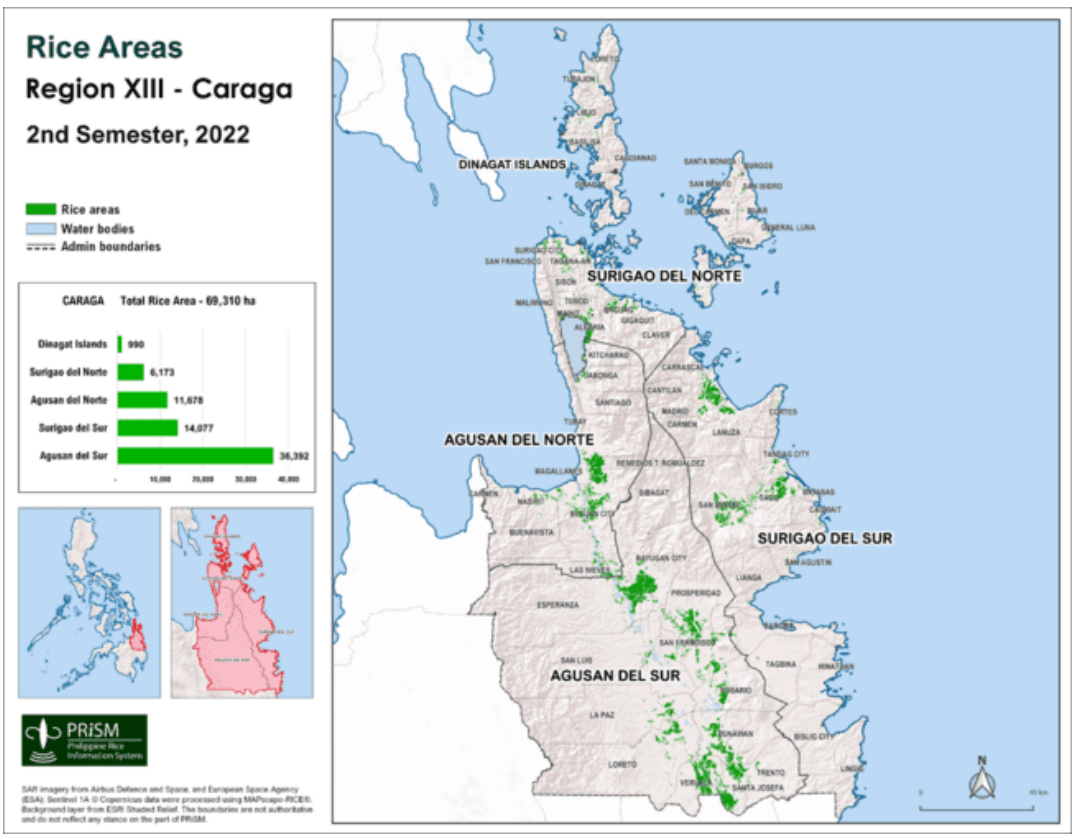

Figure 2.3 Rice Crop Map of Caraga Region Source: PhilRice

2.2.6 Flood Recovery Mapping

To evaluate the recovery of rice crops following flood damage, a series of methods were employed to analyze different growth stages of the crops. Initially, masking and overlaying techniques were used to isolate and extract the pre-flood extent of rice fields, achieved by clipping the relevant portions from the categorized flood image. This precise process identified the areas that had been flooded. Subsequently, we overlaid the pre-flood extracted rice extent onto images captured in January and February. This overlay operation enabled the distinction between regions where crops had recovered and those with limited or no recovery. Visual examination of these overlapping areas provided insights into the extent and pattern of recovery in the affected rice fields.

To quantify recovery, a straightforward mathematical calculation was applied. By comparing the areas of recovered crops to the total pre-flood rice field extent, the researchers determined the percentage of crop recovery. This metric quantified the extent to which rice crops had rebounded after the flood. Estimating post-flood rice crop recovery involves employing various techniques and rigorous analysis. The masking and overlaying techniques played a vital role in identifying flood-affected areas and assessing subsequent recovery. These methods allowed for the quantification of flood impact and offered valuable insights into the resilience and regrowth of rice crops in the affected regions.

3. RESULTS AND DISCUSSIONS

3.1 Flood Mapping

Terrain filtering in hydrology plays a critical role in extracting essential data from digital elevation models (DEMs) and assessing hydrologic features. This method involves applying diverse filters to the DEM, like slope and curvature measurements, to highlight specific topographic characteristics, aiding in the identification of hydrologic elements such as watersheds and flow directions. One widely used technique, the Digital Elevation Model-based Hydrological Analysis Utility (DEM-H), integrated into the Terrain Analysis Using Digital Elevation Models (TauDEM) software, detects water flow orientation, stream channels, and watershed boundaries. Terrain filtering is pivotal for efficient watershed management and precise floodplain mapping for identifying flooded croplands in Kitchararao Agusan del Norte. We improved DEM accuracy by addressing inconsistencies, focusing on slopes and depressions, and filling terrain sinks that hindered water outflow. Flow directions, estimated flow accumulation, and identified primary stream channels were determined, enriching the understanding of hydrological dynamics and topographical variations for flood risk assessment within the study area. Following raster calculations, non-zero values were extracted and transformed into polygon features, indicating areas susceptible to flooding based on established parameters. To comprehensively depict flood-prone regions, multiple polygon feature classes were merged into a single feature class for the area of interest. Although this combined feature class offers a visually appealing representation, additional modifications are needed to enhance accuracy. Contextual adjustments improve polygon precision by addressing boundaries and attributes. The objective was to accurately represent topography and flood hazards. Contextual modification aligns polygon boundaries and properties with topographic characteristics, enhancing accuracy. The result is a unified polygon feature class that accurately depicts flood-prone areas.

Applying a mask to the original image highlights areas prone to flooding, resulting in the masked image shown in Figure 3.1 (d). The mask is created based on predefined criteria like pixel brightness, color, or texture, which define flood-prone characteristics. This process involves filtering and identifying regions of interest in the image, isolating areas meeting the criteria for potential flooding. To create the mask, specific thresholds or image processing techniques are used to extract relevant information and highlight regions of interest in the original image. The masked image shows only the selected areas that meet the established criteria, allowing for a focused analysis of flood-prone regions. Researchers assess each pixel in the masked image by comparing its properties to the predefined thresholds. Pixels meeting or exceeding these values are highlighted as part of the flooded area. This pixel-by-pixel evaluation identifies sections that meet the conditions for potential flooding, providing valuable insights for flood mapping, disaster response planning, and mitigation strategies. Accurately delineating flooded and non-flooded regions involves determining the appropriate thresholding range through iterative testing and consideration of various factors. Initially using a default classification method, we found it overestimated the flooded area, prompting a comprehensive evaluation process to optimize the thresholding range. Binarization was employed to separate flooded and non-flooded areas based on pixel values, with iterative adjustments made to achieve optimal results. The final thresholding range was set as min-0.022 and 0.22-max, accurately distinguishing the flooded area from the non-flooded zone while minimizing false positives. This balanced approach considered specific flooding characteristics and facilitated subsequent analysis of the flooding event's extent and features, as illustrated in Figure 3.2.

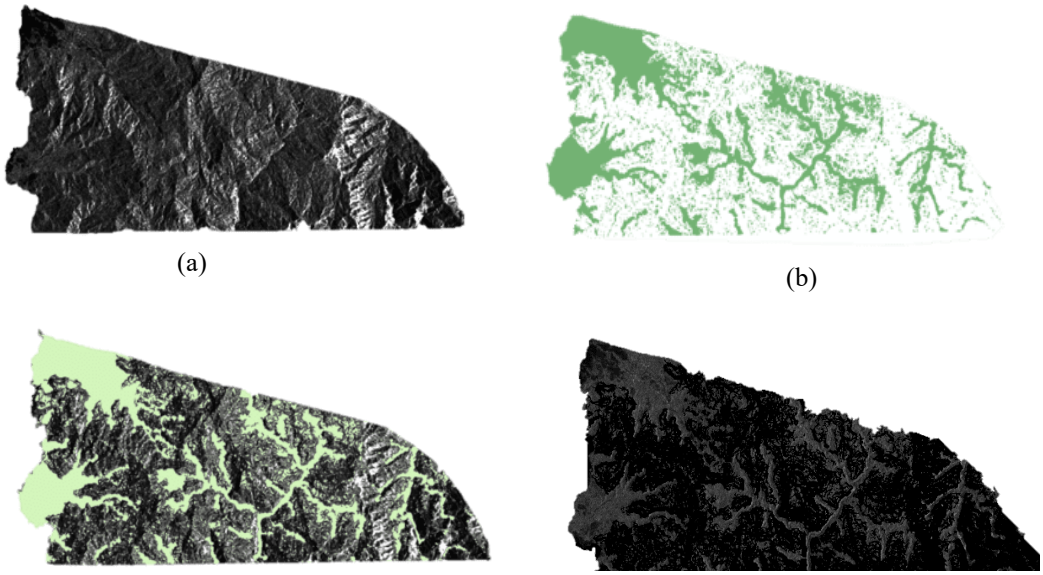

(a) (b)

(c) (d)

Figure 3.1 Process of Acquiring Image for Thresholding. (a) Pre-processed Sentinel-1, (b) Output of Terrain Filter, (c) Masking of a and b, (d) Image for Thresholding

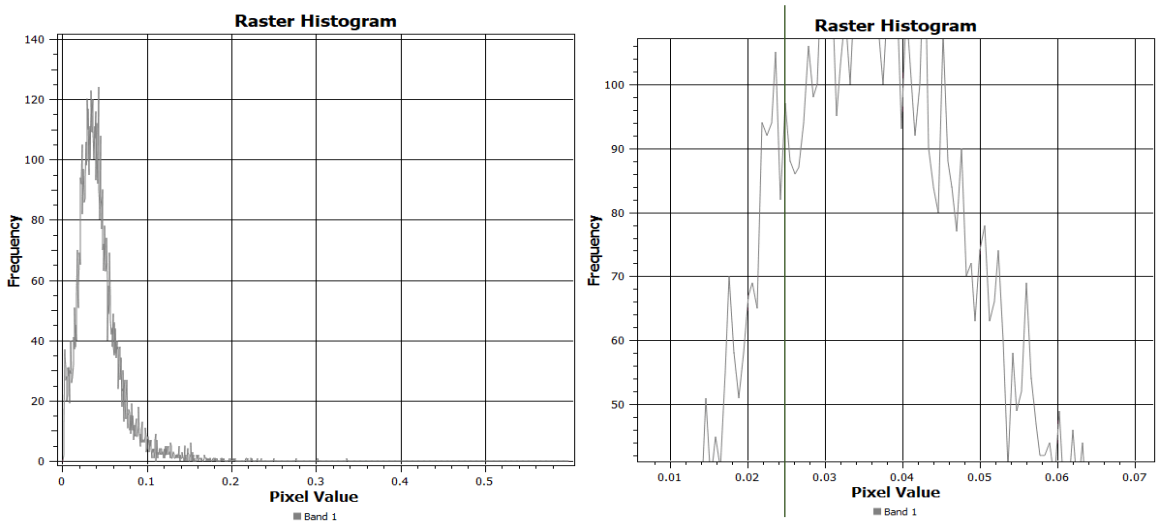

Figure 3.2 Raster Histogram of the Terrain Filtered Image

3.2 Flood and Non-Flood Accuracy Assessment

Figure 3.3 shows a map with ground truth sites used to validate flood mapping. These sites were determined through interviews with residents and damage reports from the Department of Agriculture in Kitcharao. They served as reference points for assessing the accuracy of flood mapping techniques. We compared the mapped flood extent from remote sensing data to on-site ground truth data to ensure accurate flood mapping. Table 4 provides the mean elevation values for the validation points categorized into inundated and non-inundated areas. The mean elevation for the inundated validation points is 44.71233954 ft, while the mean elevation for the non-inundated points is 47.0661427 ft. These mean elevation values served as a quantitative measure to distinguish the difference in elevation between areas affected by flooding and those unaffected. The overall accuracy of the flood map is 94% percent with kappa value of 0.88. This indicates that the method of delineating flood map passed the accuracy assessment, thus making the flood map and the method itself, reliable.

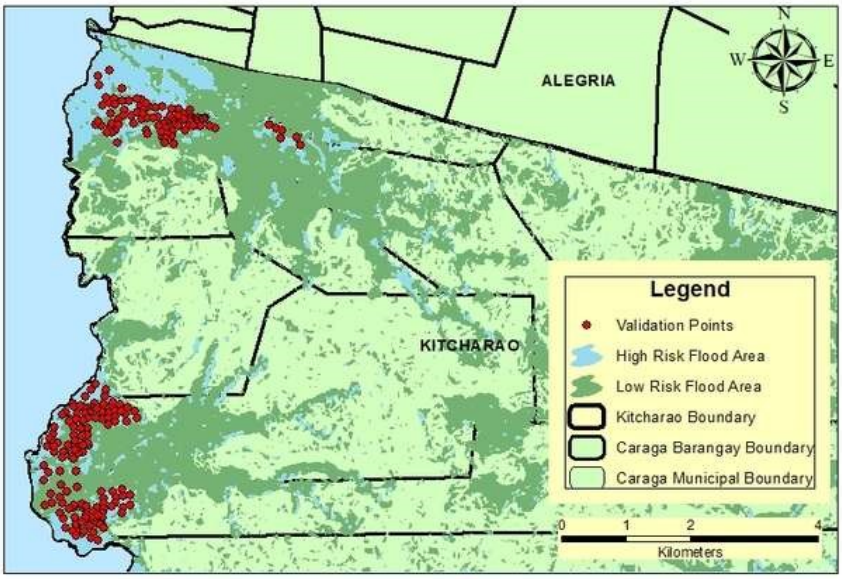

Figure 3.3 Map of the Validation Points of Flood and Non-flood areas

3.3 Rice Crop Mapping

Figure 3.4 shows the rice crop extent in December, revealing early growth stages before flooding. Figure 3.5 displays rice crops in January, highlighting those planted before flooding. Figure 3.6 depicts rice crops one month after floods, including newly planted and recovering fields. These maps provide insights into rice cultivation throughout the season and flood impacts, aiding decisions on recovery and resource management.

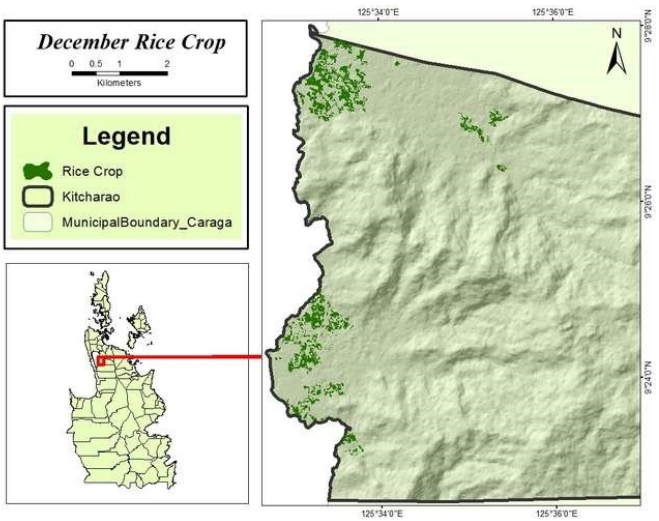

Figure 3.4 Rice Map for the month of December

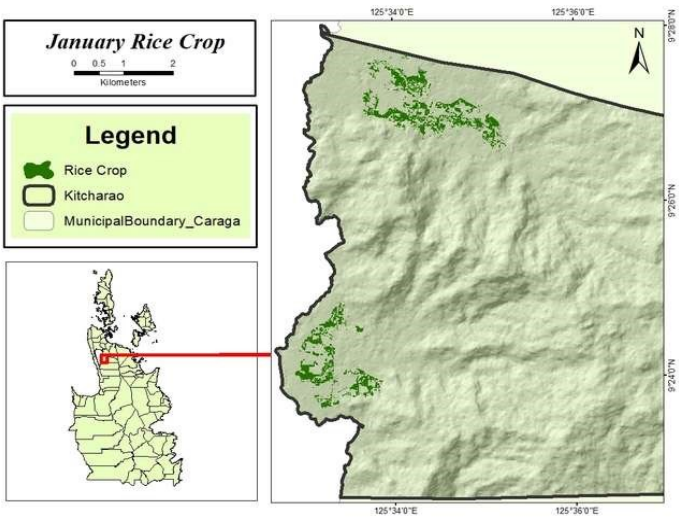

Figure 3.4 Rice Map for the month of January

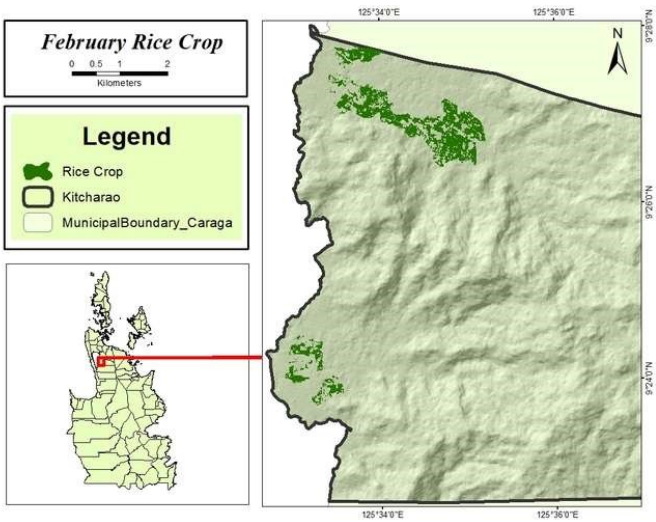

Figure 3.6 Rice Map for the month of February

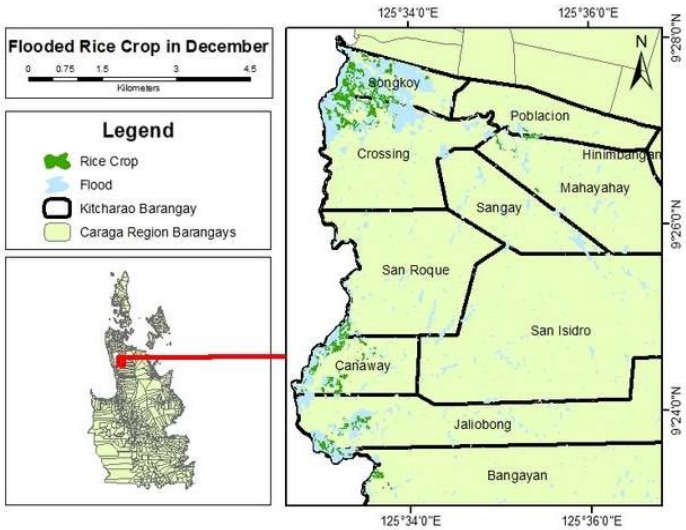

Figure 3.7 Overlaying of Flood and Non-Flood in the Boundary of Kitcharao, Agusan del Norte

3.4 Flood Recovery Mapping

Figure 3.7 depicts the boundaries of rice fields and shows the extent of flooding over these areas, illustrating the impact of floods on agriculture. It visually connects rice field boundaries with the flooded regions, enhancing understanding of flooding's effect on rice cultivation and aiding decisions in agriculture and disaster management. The findings reveal a substantial decrease in rice crop area from December (882,161.00 square meters) to January (19,880 square meters) and February (78,439 square meters), primarily due to recurrent flooding. The data show that only 2.25% of rice crops survived a week after the flooding, with a recovery rate of 8.89% after a month, indicating the prolonged impact of the flood. These results emphasize the need for effective post-flood agricultural strategies to promote crop recovery and resilience against natural disasters. The study's data can inform such strategies, emphasizing the importance of further research on flood effects on agriculture.

4. CONCLUSIONS AND RECOMMENDATIONS

The integration of optical and SAR images enhances flood damage assessment and rice crop recovery monitoring for farmers. The accuracy of the rice crop extent maps, validated with ground truth data, emphasized the reliability of the mapping method. The study revealed varying rice crop recovery across barangays, highlighting the need for tailored strategies. Combining remote sensing with ground-based data, including interviews and damage reports, provides a comprehensive understanding of recovery. This interdisciplinary approach ensures precise maps and informed decision-making in agriculture, resource allocation, and disaster management. The study showcases remote sensing's potential in post-flood crop recovery monitoring, aiding farmers and promoting flood resilience and food security in vulnerable regions. The study's results indicate that monitoring and assessing crop recovery after floods can be achieved by utilizing existing Sentinel-1 and Sentinel-2 satellite imagery along with RS and GIS techniques. It is important to acknowledge the study's limitations, particularly regarding data availability. One significant limitation is the impact of cloud cover on optical imagery, which can hinder accurate post-flood recovery assessment. Cloud cover obstructs the view of the Earth's surface and makes it challenging to analyze and validate results based solely on optical imagery. To overcome this limitation and improve the accuracy of post-flood recovery assessments, it is recommended to combine high-resolution images with ground truth data. High-resolution images provide a more detailed depiction of the terrain, enabling a more precise validation of the recovery status of agricultural lands.

5. REFERENCES

Canty, M. J. (2014). *Image Analysis, Classification and Change Detection in Remote Sensing: With Algorithms for ENVI/IDL and Python*. Taylor & Francis Group, LLC. https://books.google.com.ph/books?hl=nl&lr=&id=fGDOBQAAQBAJ&oi=fnd&pg=PP1&dq=envi+image+analysis+software+package&ots=xxNKhnDlA_&sig=kp4yN5wiGaW-dpUUR17he1dzvvM&redir_esc=y#v=onepage&q=envi image analysis software package&f=false

Conde, F. C., & De Mata Muñoz, M. (2019). Flood Monitoring Based on the Study of Sentinel-1 SAR Images: The Ebro River Case Study. *Water 2019, Vol. 11, Page 2454*, *11*(12), 2454. https://doi.org/10.3390/W11122454

Elauria, M. (2015). *Farm Land Policy and Financing Program for Young Generation in the Philippines | FFTC Agricultural Policy Platform (FFTC-AP)*. https://ap.fftc.org.tw/article/882

Guha- Sapir, D., Below, R., Hoyois, P. (2015). *EM-DAT - The international disaster database*. https://www.emdat.be/

Jha, S., Martinez, Jr. , A., Quising, P., Ardaniel, Z., & Wang, L. (2018). Natural Disasters, Public Spending, and Creative Destruction: A Case Study of the Philippines. *SSRN Electronic Journal*. https://doi.org/10.2139/SSRN.3204166

McGarragh, G., Poulsen, C., Povey, A., Thomas, G., Christensen, M., Sus, O., Schlundt, C., Stapelberg, S., Stengel, M., Grainger, D., McGarragh, G., Poulsen, C., Povey, A., Thomas, G., Christensen, M., Sus, O., Schlundt, C., Stapelberg, S., Stengel, M., & Grainger, D. (2015). SNAP (Sentinel Application Platform) and the ESA Sentinel 3 Toolbox. *ESASP*, *734*, 21. https://ui.adsabs.harvard.edu/abs/2015ESASP.734E..21Z/abstract

Nguyen, H. D., Pham, V. D., Lan Vu, P., Thanh Nguyen, T. H., Nguyen, Q. H., Nguyen, T. G., Dang, D. K., Tran, V. T., Bui, Q. T., Lai, T. A., & Petrişor, A. I. (2022). Cropland abandonment and flood risks: Spatial analysis of a case in North Central Vietnam. *Anthropocene*, *38*. https://doi.org/10.1016/J.ANCENE.2022.100341

PhilAtlas. (2015). *Kitcharao, Agusan del Norte Profile*. https://www.philatlas.com/mindanao/caraga/agusan-del-norte/kitcharao.html

Pinlac, B. (2022). *Agricultural damage from recent floods in Mindanao, Luzon now at P37.68M | Inquirer News*.

Torres, R., Navas-Traver, I., Bibby, D., Lokas, S., Snoeij, P., Rommen, B., Osborne, S., Ceba-Vega, F., Potin, P., & Geudtner, D. (2017). Sentinel-1 SAR system and mission. *2017 IEEE Radar Conference, RadarConf 2017*, 1582–1585. https://doi.org/10.1109/RADAR.2017.7944460

Wu, T., Luo, J., Fang, J., Ma, J., & Song, X. (2018). Unsupervised object-based change detection via a weibull mixture model-based binarization for high-resolution remote sensing images. *IEEE Geoscience and Remote Sensing Letters*, *15*(1), 63–67. https://doi.org/10.1109/LGRS.2017.2773118